PCP
PLANT & CELL PHYSIOLOGY

A Cellulose Synthase-Containing Compartment Moves Rapidly Beneath Sites of Secondary Wall Synthesis

Raymond Wightman, Robin Marshall and Simon R. Turner*
Faculty of Life Sciences, University of Manchester, Manchester M13 9PT, UK

Regular Paper

The woody secondary walls of plants represent the major sites of cellulose deposition. The polymerization of cellulose occurs at the plasma membrane by the secondary wall cellulose synthase complex (CSC). In the long, cylindrical cells that make up the xylem, secondary wall deposition is confined to discrete regions of the cell, and yellow fluorescent protein (YFP)-labeled CSCs are also localized to these regions. Using fluorescence loss in photobleaching (FLIP) of complete hoops containing YFP–CSCs, we demonstrate movement of the complexes beneath the nascent secondary wall in developing xylem vessels. We have devised a method for determining particle velocities for particles moving around a cylindrical object using data from FLIP. By applying this method to the hoops of YFP–CSCs of the developing vessels, we have obtained the first estimates of speed of these complexes. These speeds are calculated to be in excess of 7 μm s^{-1} and are far higher than those speeds previously reported for the primary wall complex. These high speeds are unlikely to be consistent with CSC movement being attributed to cellulose synthesis alone, and suggest the existence of a highly motile compartment beneath the nascent secondary wall.

Keywords: *Arabidopsis* • Cellulose synthase complex • FLIP • Secondary cell wall • Xylem • YFP.

Abbreviations: CFP, cyan fluorescent protein; CSC, cellulose synthase complex; DCB, dichlorobenzonitrile; DMSO, dimethylsulfoxide; ER, endoplasmic reticulum; FLIP, fluorescence loss in photobleaching; FRAP, fluorescence recovery after photobleaching; YFP, yellow fluorescent protein.

Introduction

Cellulose is the world's most abundant biopolymer and serves as an important global sink for carbon. It is synthesized by a large 30 nm multiprotein complex called the cellulose synthase complex (CSC) (Mueller and Brown 1980). The CSC is visualized within the plasma membrane as a six-lobed rosette structure. It is thought that each complex synthesizes one cellulose microfibril and that each microfibril consists of the order of 36 glucan chains (Somerville 2006). The only known components of the CSCs are the CesA proteins that are believed to be the catalytic subunits, each polymerizing a single glucan chain (Taylor et al. 2003).

It is believed that the CSC moves through the plasma membrane as it adds glucose units to the growing cellulose microfibril, guided by the underlying microtubules (Hepler and Newcomb 1964, Delmer and Amor 1995). There is evidence suggesting that this polymerizing activity supplies the force for movement of the 30 nm complex. First, bacteria have been observed to move through the growth media as they extrude cellulose (Herth 1980). Secondly, velocities of yellow fluorescent protein (YFP)-labeled primary wall CSCs have been shown to be similar before and after the drug-induced removal of microtubules, indicating that microtubule-associated proteins, such as motor proteins, are not responsible for powering movement of the complex (Paredez et al. 2006, DeBolt et al. 2007a).

As the major component of woody secondary walls, cellulose provides much of the mechanical stability of plants. In fully differentiated xylem vessels, the secondary walls exhibit a characteristic pattern and serve to withstand the large negative pressures associated with water transport. The secondary wall CSC contains an exclusive set of three CesA proteins that were identified in a forward genetic

*Corresponding author: E-mail, simon.turner@manchester.ac.uk; Fax, +44-161-275-3938.

Plant Cell Physiol. 50(3): 584–594 (2009) doi:10.1093/pcp/pcp017, available online at www.pcp.oxfordjournals.org

screen for *Arabidopsis* mutants displaying an *ir*regular *x*ylem (*irx*) phenotype. The three CesA subunits, IRX1, IRX3 and IRX5, are all required for correct assembly of the secondary wall CSC and plasma membrane localization (Turner and Somerville 1997, Taylor et al. 1999, Taylor et al. 2000, Gardiner et al. 2003, Taylor et al. 2003). Live imaging of the secondary wall complex in developing vessels has been reported using a fusion between YFP and IRX3 (Wightman and Turner 2008). YFP–IRX3 localizes to sites of secondary wall deposition, and its maintenance at the cell periphery is dependent upon the thick bands of cortical microtubules. To date, YFP–IRX3 movement directly below the secondary thickenings has not been demonstrated.

Several methods exist for studying diffusion-based movement within membranes using fluorescently labeled particles. Of these, fluorescence recovery after photobleaching (FRAP) and fluorescence loss in photobleaching (FLIP) are the most common. Both methods involve bleaching an area of interest. For FRAP, a short bleaching period followed by post-bleach acquisitions is used to measure any recovery of fluorescence into the bleached area by non-bleached particles (Reits and Neefjes 2001). In FLIP, a prolonged bleaching period is used and movement of bleached particles outwards from the bleached region is measured (White and Stelzer 1999). Most studies using these techniques have measured diffusion-based movement within membranes rather than the type of powered movement that is expected to be exhibited by the CSC (Axelrod et al. 1976, Wey et al. 1981, Cole et al. 1996). In plants, FRAP has been used successfully to explore changes in mobility of a leucine-rich receptor kinase at the plasma membrane (Ali et al. 2007), and both FRAP and FLIP have been used to demonstrate regulated movement of splicing factors (Ali and Reddy 2006).

Using FLIP of YFP–IRX3, we demonstrate movement of the CSCs at the sites of secondary wall synthesis. We describe a novel method for calculating particle velocities around a complete hoop during FLIP. By applying this method to bands of YFP–CSCs we have calculated their speeds to be in excess of 7 μm s^{-1}. Such rapid movement is unlikely to be solely due to the CSCs making cellulose microfibrils and suggests that a novel mechanism exists for movement of the CSC at sites of secondary cell wall deposition.

Results

Application of FLIP to examine CSC movement beneath the sites of secondary wall formation

Previous work has shown fluorescent protein fusions with the N-terminus of IRX3 to functionally complement an *irx3* mutant line (Gardiner et al. 2003). In roots of 5-day-old seedlings, YFP-labeled IRX3 (YFP–CSCs) can be clearly observed in the developing xylem vessels. Using a confocal microscope, bands of YFP–CSCs can be seen to be arranged in hoops and spirals (**Fig. 1**) as previously described (Wightman and Turner 2008). Due to the likely high density of YFP–CSCs within these bands, ranging from 60 to 200 CSCs μm^{-2} for complexes residing at the plasma membrane (Herth 1985, Haigler and Brown 1986, Schneider and Herth 1986), the focal depth required for imaging and the presence of air pockets within the root, individual particles cannot be distinguished from one another. Consequently, it is not feasible to track individual particles using rapid confocal time-lapse movies. Attempts to monitor movement of the CSCs using FRAP proved unsuccessful. Small bleached regions resulted in recovery prior to the first post-bleach scan, and large bleached regions resulted in loss of signal of the whole hoop, presumably due to rapid movement of particles into and out of the region during bleaching (data not shown). While rapid movement of rosettes may make FRAP impractical,

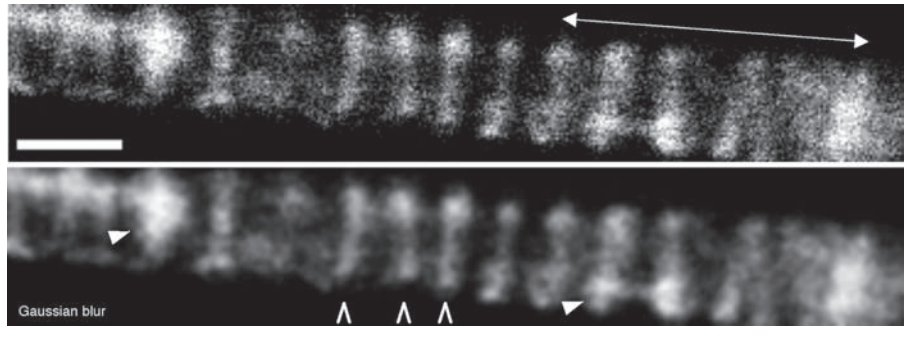

Fig. 1 YFP-labeled CSCs in developing xylem vessels. Average of two confocal scans showing a portion of a developing xylem cell (top panel). The direction of the long axis of the cell is shown above. For clarity, a 2 pixel radius Gaussian blur was applied to the image and is shown in the lower panel. Filled arrowheads indicate examples of intracellular organelles that contain YFP–CSCs and are transported around the long axis of the cell (Wightman and Turner 2008). Barbed arrowheads show the positions of bands of YFP–CSCs at sites of secondary wall synthesis. Bar = 5 μm.

these observations suggested that a FLIP approach to study CSC movement might be feasible.

With this approach, each confocal scan included a portion where the laser was increased and used to generate a bleach zone in a selected region of the hoop of interest. Any YFP–CSCs that passed through the bleach zone when it was applied would be photobleached. These bleached CSCs subsequently moved around the hoop effectively decreasing the fluorescence signal in the rest of the hoop. Each FLIP experiment consisted of one pre-bleach scan followed by 40 FLIP scans and then 10 or 20 post-bleach scans. Loss of fluorescence signal from the hoop was monitored relative to the loss of signal across the whole image due to general acquisition bleaching. Loss of fluorescence during FLIP from the bleached hoop generally occurred much more rapidly than in comparable regions outside of the hoop under study. Average projections of the first 10 FLIP scans and the last 10 FLIP scans were calculated (**Fig. 2a**). Mean pixel intensities of the FLIP hoop (minus the bleached area) and a non-bleached hoop were normalized to general acquisition bleaching and then plotted. The FLIP hoop intensity dropped significantly compared with the non-bleached hoop, showing that YFP–CSCs are constantly moving around the hoop. With each scan the number of bleached CSCs should be proportional to the width of the bleached area. This prediction is supported by the experiment shown in **Fig. 2b**. A wider bleach zone results in a more rapid degradation of the hoop fluorescence signal as the YFP–CSCs are

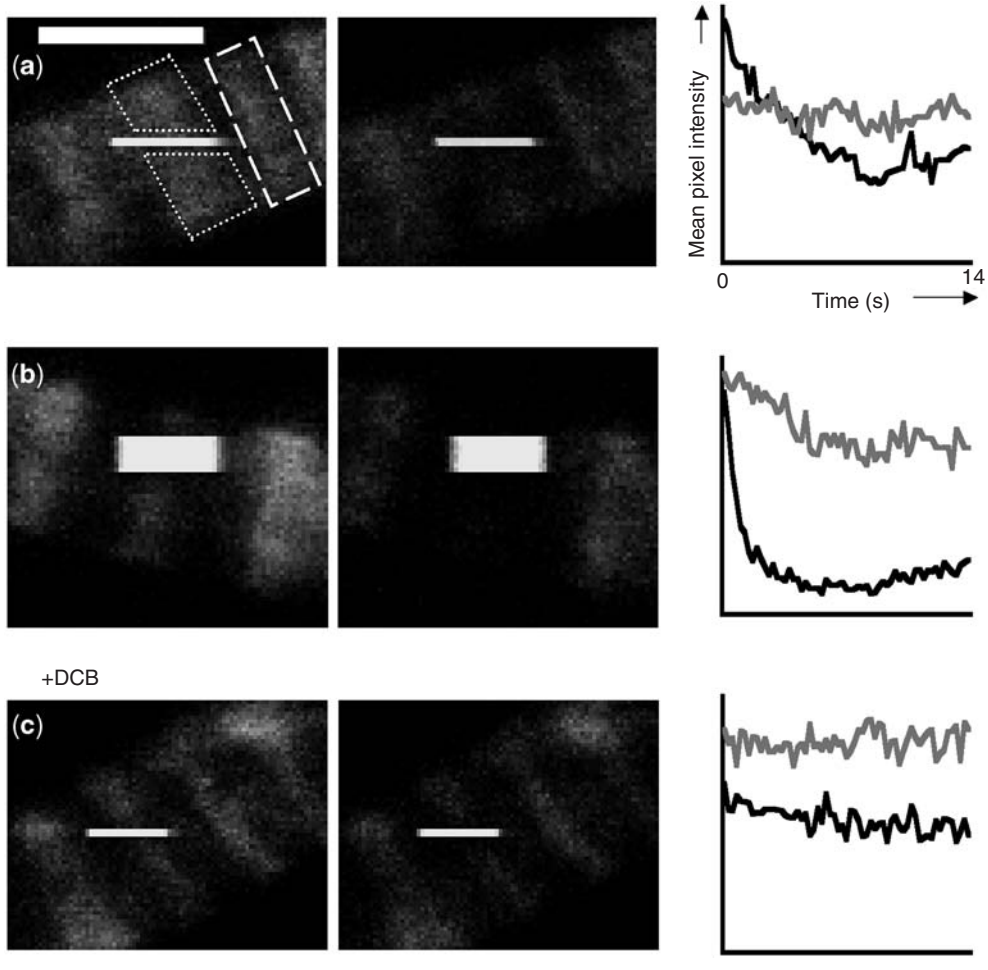

Fig. 2 Using FLIP to demonstrate CSC movement. An average of 10 confocal scans are shown at the beginning (left panels) and end (middle panels) of the time course during FLIP. Measurements were taken of the hoop undergoing FLIP (dotted region of interest) and of an unbleached hoop (e.g. dashed region of interest). The line plots (right panels) show the mean hoop pixel intensities measured during the experiment for the FLIP hoop (black lines) and the unbleached hoop (gray). The results were normalized to general acquisition bleaching. For experiment (a), a bleach line 2 pixels wide results in fluorescence decay of the whole hoop compared with a hoop with no bleach line. A wider bleach line, as shown in (b), is seen to result in more rapid fluorescence decay. Treatment with the cellulose inhibitor DCB (c) results in minimal fluorescence decay. Bar = 10 µm.

more rapidly photobleached (**Fig. 2b** and **Supplementary Movie S1**). In all FLIP experiments the intensity of the hoop fluorescence never decreased to zero even though the curve appears to flatten out well before the end of the experiment (as shown in **Fig. 2b**).

Direction of CSC movement

It has been demonstrated that, for the primary wall CSC, movement along a single path occurs bidirectionally (Paredez et al. 2006). To determine the directionality of YFP–CSC movement during secondary wall synthesis, FLIP was carried out on a hoop, and fluorescence intensity was compared within the regions flanking the bleach zone. If the YFP–CSCs are moving in a single direction around the hoop, fluorescence should decrease preferentially on one side of the bleach zone. Three-dimensional (3D) color surface plots of confocal FLIP scans show that FLIP appears to be taking place equally either side of the bleach zone (**Fig. 3**). This is supported by the series of profile plots in **Supplementary Movie S2** that show identical rates of fluorescence loss on either side of the bleach zone. The data suggest the YFP–CSCs are moving bidirectionally around the hoops.

Treatment with an inhibitor of cellulose synthesis slows movement of the CSCs

To see if we could detect any change in CSC motility, we looked at the effect of pre-incubating the seedling with the cellulose synthesis inhibitor, dichlorobenzonitrile (DCB), 30 min prior to carrying out the FLIP analysis. DCB has recently been shown to aggregate and slow the movement of the primary wall complex, observed as a YFP–CesA6 fusion, at the cell cortex (DeBolt et al. 2007b). When a bleach zone was applied across a hoop, minimal loss of fluorescence due to FLIP was observed compared with a neighboring hoop (**Fig. 2c**). Measurements of the hoop intensity showed a slow decay curve compared with that of an untreated seedling (compare plots for **Fig. 2c** with a).

To have any effect upon developing vessels, DCB needs to penetrate deep within the root tissues. This means the ability of DCB to infiltrate the stele region will determine the extent of fluorescence decay. Across multiple experiments, the effect of DCB upon FLIP of the hoops, as shown by the decay curves of **Fig. 4**, showed some limited overlap with those of untreated seedlings. Despite this overlap, after 40 scans, on average DCB-treated seedlings exhibited decreased fluorescence loss due to FLIP compared with the untreated controls. For the untreated controls with a bleach width of ≤2 pixels ($n = 7$), fluorescence intensity at the end of FLIP was 44% of the initial intensity (SE ± 3%). In DCB-treated seedlings ($n = 9$), this figure rose to 63% (SE ± 4%). Both a Student's *t*-test ($P = 0.0026$) and a Mann–Whitney–Wilcoxon test ($P = 0.0034$) showed that these differences are significant (see Materials and Methods). Furthermore, in >15 FLIP experiments on untreated seedlings, no curve similar to that shown in **Fig. 2c** was observed. The data indicate, therefore, that DCB slows the movement of CSCs beneath the regions of secondary wall formation

A method for determining particle velocities around a hoop

To determine the velocity of the CSCs under non-inhibiting conditions, measurements were taken of the mean pixel intensity (I) together with the bleach zone width (d) and hoop radius (a), for several cells. Longitudinal transport of YFP–CSCs in large organelles, which include the Golgi, occurs along the whole length of the cell (Wightman and Turner 2008) and affects the measurement of hoop fluorescence decay during FLIP. For this reason, only bands with no visible intracellular organelles passing beneath or in close proximity were selected for analysis. An illustration of the experiment

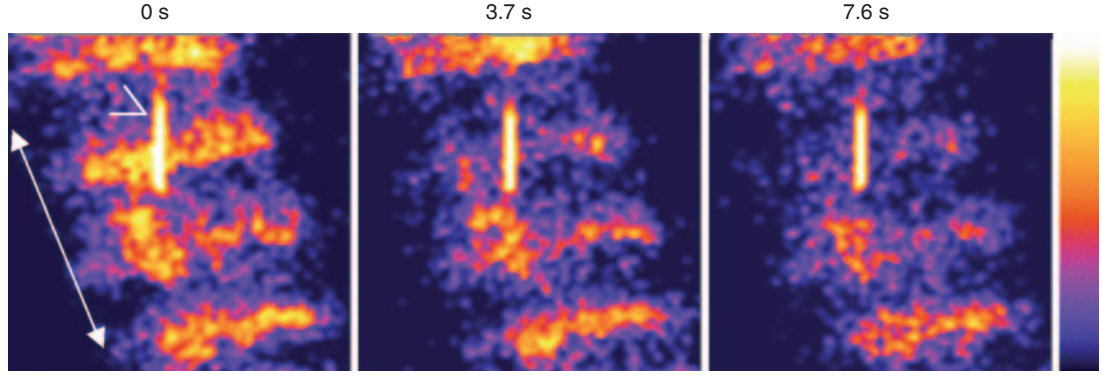

Fig. 3 CSC movement around the hoop is bidirectional. Surface plots of stills taken from an image sequence of FLIP from an untreated seedling. The filled arrow indicates the long axis of the cell. The arrowhead points to the bleach line. The entire image sequence is available as **Supplementary Movie S2**.

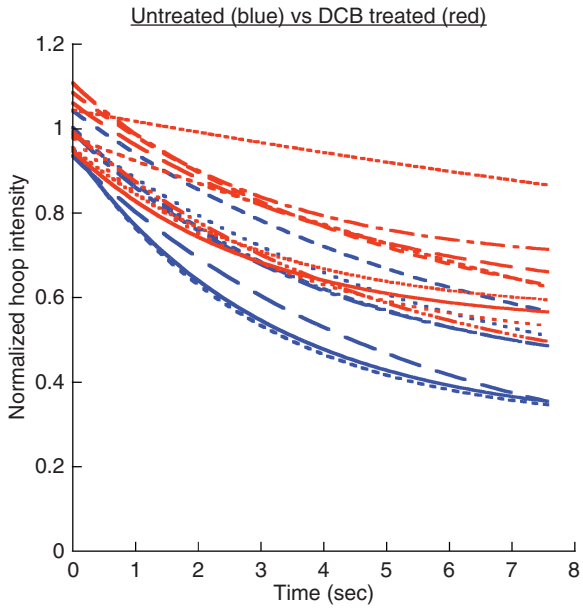

Fig. 4 Fluorescence decay during FLIP for untreated and DCB-treated seedlings. Shown are all plots of fluorescence decay for each treatment. The bleach zone width was ≤2 pixels. The decay after DCB treatment ($n = 9$) is generally slower than observed for the decay curves for untreated seedlings ($n = 7$).

is shown in **Fig. 5**. The time taken for one confocal scan (τ) was 0.194 s. The proportion that is lost with each scan is a function of the width of the bleach zone relative to the diameter of the cell and the number and velocity of CSCs re-entering the bleach zone after each scan. The loss of fluorescence is given by the formula:

$$I(t) = I_o\left(1-\frac{d}{\pi a}\right)\left(1-\frac{v\tau}{\pi a}\right)^{(i-1)} + B_s \qquad (1)$$

where I_0 is the mean pixel intensity of the first scan, $I(t)$ is the mean pixel intensity of the ith scan (i.e. scan number 2, 3, 4 etc..), v is the velocity of the CSC, d is the width of the bleached area measured around the curved surface of the cell, a is the radius of the cell and B_s is the constant background due to either stationary/very slow moving CSCs or a small amount of cell wall autofluorescence. The derivation of this formula is described in **Supplementary Fig. S1**. In **equation (1)**, the first term in parentheses represents the first bleach when fluorescence loss always depends upon geometry alone rather than CSC velocity.

For FLIP experiments, where the bleach zone area is fully replenished with CSCs between each bleach, the loss of fluorescence should follow a simple power law in which the same proportion of fluorescence is lost with each scan. In our case, this loss of fluorescence can readily be expressed

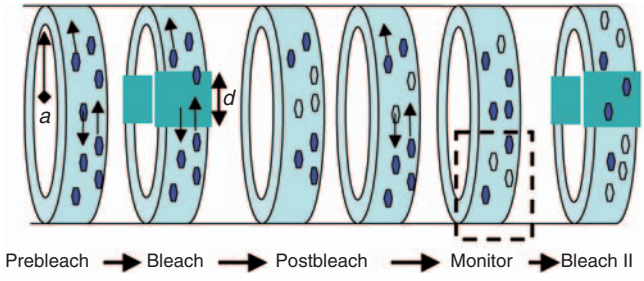

Fig. 5 Using FLIP to calculate particle velocities. YFP-labeled particles (blue) move around a band with radius a ('Prebleach'). The bleach zone, of width d, is applied and bleaches all particles within this region ('Bleach'). Movement of bleached particles out of the bleach zone is coupled with movement of both non-bleached and previously bleached particles into the zone ('Postbleach'). Measurements of average fluorescence intensity of the regions of the band outside the bleach zone are taken ('Monitor'). The process is then repeated ('Bleach II').

in terms of the bleach gap (d) and velocity (v). It is equivalent to the decay constant (lifetime) in, for example, radioactive decay. Our data are consistent with this simple interpretation.

The speed, v, can only be measured if it is lower than a maximum calculatable speed (v_0) given by the formula:

$$v_o = \frac{d}{\tau} \qquad (2)$$

If the actual speed is greater than this, then v_0 represents the minimum speed and simply tells us that the speed is at least that required to refill the bleach gap. A real example is given in **Fig. 6c** and shows the excellent fit between the loss of fluorescence intensity with time and geometric curves, consistent with fluorescence decay following a power law. The ability to measure actual speeds is achieved by using larger bleach widths such that the bleached area will not become completely repopulated between successive scans. For experiments which have a velocity less than v_0, the bleach width can be calculated by substituting $v = d'/\tau$ in **equation (1)** which now becomes:

$$I(t) = I_o \exp\left[\frac{1}{\tau}\ln\left(1-\frac{d'}{\pi a}\right)\right]t + B_s \qquad (3)$$

where d' is now the apparent bleach width. Using the FLIP data this formula allows us to calculate the apparent bleach width. A plot of the apparent bleach width [derived by fitting the data to **equation (3)**] vs. the measured bleach width (derived from the confocal specifications) will give a straight line of unit slope for those experiments where $v > v_0$. When $v < v_0$, the value for the calculated bleach width will be less

than the measured bleach width and an actual velocity can be determined by inserting the calculated value d' for d into **equation (2)**.

Fluorescence decay data from FLIP experiments with small (<0.5 µm), medium (~1.5 µm) and large (>2 µm) width bleach zones were used to determine the calculated bleach zone width. A plot of the apparent vs. measured bleach widths showed that the values for small- and medium-sized bleach zones fit a straight line that intercepts close to zero (**Fig. 6a**). This means that the CSC velocities are above the maximum measurable velocity, v_0 Consequently, for bleach zone widths of up to 1.5 µm, $v > v_0$, the CSCs must be moving at velocities >6 µm s^{-1}. The two large bleach zone experiments with measured widths of 2.2 and 3.3 µm gave apparent bleach width values that were significantly lower than for the corresponding measured geometric values. This indicates that $v < v_0$ and so **equation (2)** can be used to calculate CSCs moving at speeds of 9.14 (±0.72) µm s^{-1} and 8.13 (±0.50) µm s^{-1}, respectively. The fluorescence decay curve for the hoop containing a 3.3 µm bleach zone is shown in **Fig. 6b,** together with an expected curve fit if the decay were geometric (i.e. if $v > v_0$). A decay curve for a hoop containing a more narrow bleach zone (1.3 µm) is shown for comparison (**Fig. 6c**) and is seen to match the geometric curve closely.

The fast moving particles represent CSCs located at the cell periphery

The rapidly moving complexes could represent a location within or neighboring the plasma membrane or, alternatively, could represent a more internal location within the cytoplasm. To investigate the spatial distribution of the bands of CSCs within the developing vessel, YFP–CSCs were viewed along with cyan fluorescent protein (CFP)-labeled microtubules. A confocal section of the upper surface of a developing vessel shows bands of cortical microtubules (**Fig. 7a**) and bands of YFP–CSCs (**Fig. 7b**) as previously described (Wightman and Turner 2008). By moving the focal plane to the center of the cell, the bands can be seen to be located at the periphery (**Fig. 7c**). Line profiles were plotted from two regions of interest that begin outside the cell and end within the cytoplasm (**Fig. 7d**). The profiles (**Fig. 7e**) from region 1 show YFP–CSCs (green) and CFP–microtubules (red) to overlap fully. In region 2, the YFP fluorescence is observed to be periphery-proximal to the microtubules; however, the resolution limit of the optics (approximately 200 nm) means that the signal could originate from either within the plane of the plasma membrane or directly beneath. A similar analysis was performed for YFP–CSCs together with an endoplasmic reticulum (ER) reporter (**Supplementary Fig. S2**). The ER, occupying space within the cytoplasm, was chosen because the network can extend close to the cell surface (**Supplementary Fig. S2**). The bands of CSCs were found to be periphery-proximal to the ER network. The data show, therefore, that CSCs within hoops occupy a peripheral compartment of the developing vessel.

Discussion

While high rates of localized cellulose deposition in xylem cells have many advantages for studying cellulose synthesis, the very high density of rosettes in regions of secondary cell wall deposition makes the resolution of individual CSCs unlikely. Furthermore, even in the roots of *Arabidopsis* seedlings, developing xylem vessels are located several cell layers from the outside of the root, and these intervening cell layers and air within the cell walls contribute to distorting the microscope image, making very high resolution microscopy challenging. The initial aim was to use FRAP to study movement of the rosettes, but recovery was either too rapid to visualize the bleached area or the entire band became bleached. The obvious interpretation of these results is that the CSCs are moving very rapidly around the hoops. In order to determine how quickly the CSCs might be moving, we have derived a formula for calculating particle velocity using the fluorescence decay measurements taken from FLIP experiments. This formula can be applied to any rapidly moving and bleachable particles that move around a cylindrical object in a complete hoop. Using these equations, we were able to calculate particle velocities for YFP–CSCs that move in a complete ring around the surface of a developing xylem cell. The data (**Fig. 6**) suggest that up to a bleach zone width of 1.3 µm the decay follows a power law, which can be readily expressed in exponential form [see **equation (3)**]. This behavior occurs if the bleach zone is completely repopulated with unbleached rosettes between scans. The relationship appears to hold with a bleach zone width of up to 1.3 µm that would correspond to a minimum speed of nearly 7 µm s^{-1}. For these smaller bleach widths, a plot of the calculated width vs. the measured width was found to fit a straight line, intercepting close to zero. The y-intercept value represents the small amount by which the confocal laser beam extends beyond 1 pixel. For two experiments with a measured bleach zone of >1.3 µm, the calculated bleach zones were found not to fit the line, meaning these experiments could be used to determine particle velocity. The actual velocities were calculated to be 8.13 (±0.50) and 9.14 (±0.72) µm s^{-1}, the two measured values being equal within errors. These figures could represent average velocities as CSCs may be moving at a range of speeds.

Our estimates of speed, based upon calculations using the FLIP data, correspond to polymerization rates of approximately 17,000 glucose units per glucan chain s^{-1} for plasma membrane-localized particles, much higher than the 16 units s^{-1} reported by Paredez et al. (2006). Based on our calculated speeds, we can estimate the total time it would take

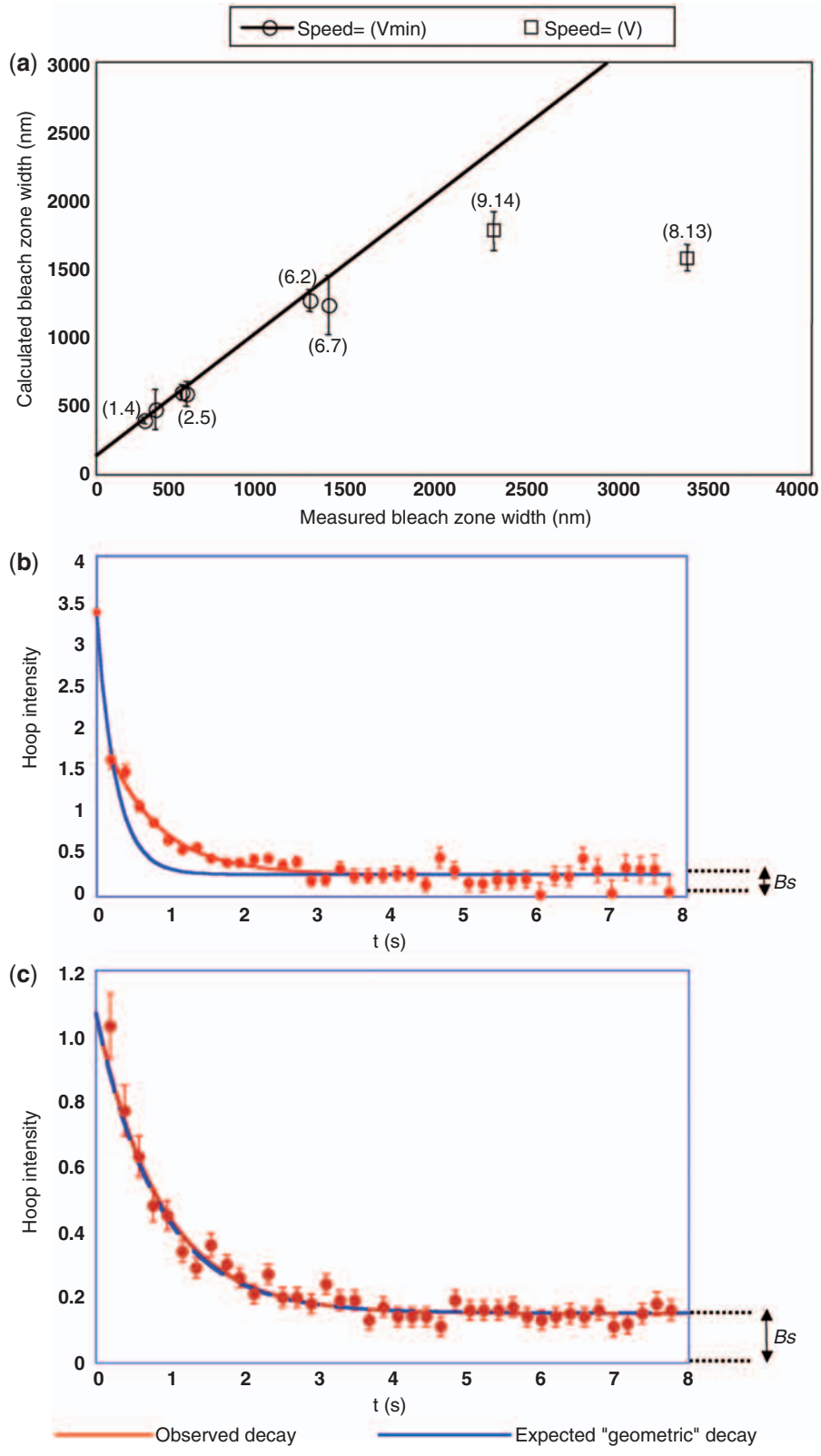

Fig. 6 Calculating velocities of CSCs. Hoop fluorescence decay was used to calculate the theoretical bleach zone width (*d*) using the formula described in the text and in **Supplementary Fig. S1**. (a) A plot of calculated (theoretical) *d* against measured *d*. For measured bleach zone widths of ≤1.3 µm, calculated values fit a straight line as shown. The minimum velocity, v_0, is shown in parentheses. For bleach zones with

to complete cellulose deposition at the secondary wall. Our calculation is as follows: for a typical cell of 10 µm in diameter the circumference is 31 µm. The secondary cell wall is around 1 µm thick and, assuming a unit size of around 5 nm for a microfibril, it would be equivalent to approximately 200 layers of microfibrils. Several studies have reported the density of individual rosettes within the plasma membrane beneath secondary thickenings from freeze-fracture preparations of developing xylem vessels. No measurements have been reported for *Arabidopsis*; however, two values of 191 rosettes µm^2 (Herth 1985) and 135 rosettes µm^2 (Schneider and Herth 1986) have been reported as the maximum rosette density in *Lepidium sativum*. For maize, the maximum density is reported to be significantly lower at 93 rosettes µm^2 (Schneider and Herth 1986). In differentiating cells of cultured *Zinnia elegans*, a figure of 65 rosettes µm^2 has been reported during the early stages of secondary wall formation (Haigler and Brown 1986). For the following purposes, we will use a figure of 100 rosettes µm^{-2}. This means, for our estimates, there are 3.1×10^3 rosettes within the plasma membrane beneath a complete hoop of width 1 µm. Assuming a minimum speed of 7 µm s^{-1} for a single CSC, the area of microfibrils deposited in 1 s equals 108.5 µm^2 [(3.1×10^3 CSCs) × (7 µm s^{-1}) × (5×10^{-3} µm microfibril unit size)]. As deposition is confined to the complete hoop of area 31 µm^2, a single monolayer will be synthesized and deposited in just 0.3 s, with completion of synthesis of the 200 layers taking <1 min. Although the assumptions of rosette density and the even distribution of CSCs may not be accurate, differing densities are unlikely to alter this figure significantly. Therefore, these estimates appear high if derived solely from particles moving through the plasma membrane as they make cellulose. Although the bands of CSCs are clearly observed to be located at the cell periphery (**Fig. 7**), the limitations of resolution mean we cannot distinguish particles at the plasma membrane from those in the cytoplasm directly below the bands. Previously, we have shown movement of intracellular YFP–CSC-containing compartments along the long axis of developing xylem vessels (Wightman and Turner 2008). It is feasible to suggest that a subset of these compartments switch to local movement around and beneath the growing secondary walls. It would be expected, therefore, that the region directly below the secondary thickening would consist of CSCs at the plasma membrane and CSCs packed within a population of small organelles or vesicles

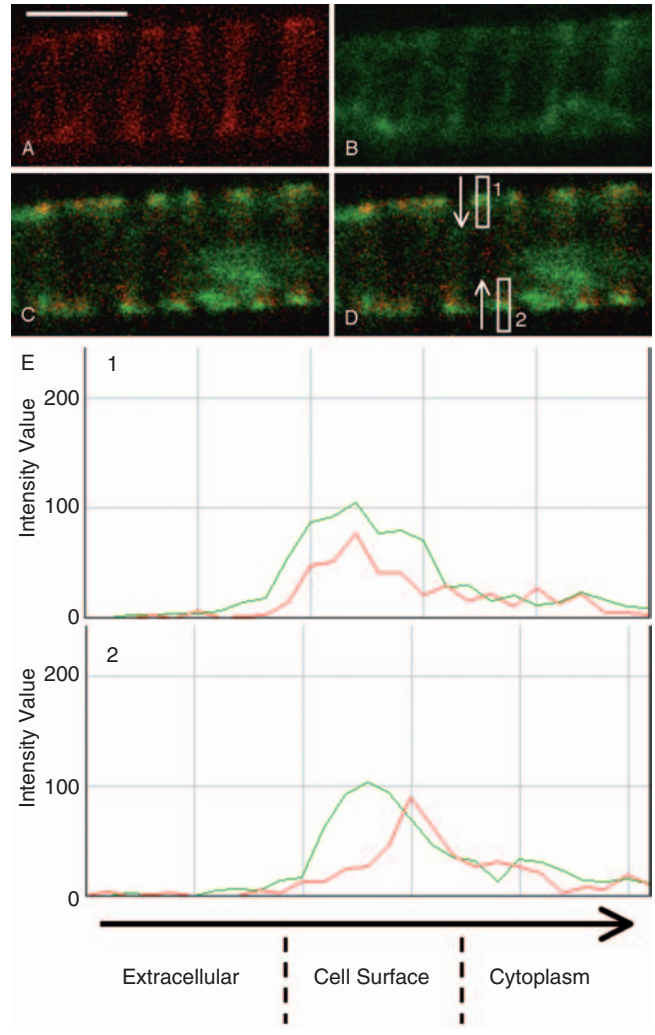

Fig. 7 Hoops of YFP–IRX3 are located at the cell surface. *Arabidopsis* line RWYC2, which expresses both *YFP–IRX3* and a CFP–microtubule reporter, was used to examine the spatial distribution between bands of CSCs and the cortical microtubules using a confocal microscope. (A) Upper surface of a developing xylem vessel showing bands of CFP-labeled microtubules. YFP–IRX3 (CSC) is shown in (B). (C) The same region of the developing vessel viewed at a focal plane that transects through longitudinally. The hoops of microtubules (red) and CSCs (green) are located at the edges of the cell. Two regions were selected for further analysis (D) and line profiles were plotted (E). The arrows in (D) represent the direction of the profiles in (E) so that the plots begin from the outside of the cell (left) to inside (right). The data show the bands of CSCs to be in very close proximity to the cortical microtubules.

widths >1.3 µm, calculated *d* values do not fit the line; therefore, these experiments will exhibit a solvable velocity (shown in parentheses). The errors were calculated by propagating the random statistical fluctuations on the measured intensities via the exponential fit. (b) A geometric fluorescence decay curve where measured bleach width equals calculated width is shown in blue. Observed hoop fluorescence decay gives a less steep decay (shown in red) indicating that a velocity can be determined. This velocity was calculated as 8.13 (±0.50) µm s^{-1}. *Bs* represents the 'constant' background of autofluorescence or stationary CSCs. The error bars represent the random statistical fluctuations in intensity measurement. For comparison, a decay curve for a narrower (1.3 µm) bleach zone is shown in (c) and is observed to be identical to the curve representing geometric decay.

within the cytoplasm. From observations of electron micrographs of developing xylem vessels in sycamore, Wooding and Northcote (1964) reported the existence of compartments, presumed to be Golgi-derived vesicles, closely associated with the secondary thickenings. Further work, by Haigler and Brown (1986), has found rosettes to reside in vesicles that appear to be undergoing fusion with the plasma membrane below the secondary thickening. These compartments are good candidates for the fast moving particles measured during FLIP. This means there are potentially three different populations of CSCs existing within different compartments within the developing vessel: (i) at the plasma membrane beneath secondary thickenings; (ii) in organelles moving longitudinally along actin cables; and (iii) in cortical vesicles that move rapidly and are restricted to the area beneath secondary thickenings. The existence of CSCs within the first two compartments has been previously demonstrated by the freeze-fracture studies and the live imaging described above. The third compartment is inferred from the high speeds measured during FLIP. The spatial distribution of CSCs, which includes the position of the possible third compartment, in relation to the secondary wall is summarized in **Supplementary Fig. S3**.

In an attempt to look for perturbations in CSC movement we made use of the chemical inhibitor of cellulose synthesis, DCB. Another inhibitor, isoxaben, was not found to be useful for FLIP analysis since it results in disappearance of the bands. Likewise, the disruption of microtubules or actin after treatment with oryzalin or lantrunculin, respectively, also results in band removal and therefore no targets exist for FLIP analysis (Wightman and Turner 2008). The mode of DCB action, in primary wall formation, has been shown to be the cessation of CSC movement within the plane of the plasma membrane. In the presence of DCB, these primary wall CSCs appear to aggregate at sites within the plasma membrane and these sites may represent insertion sites of the CSCs from an intracellular compartment (DeBolt et al. 2007b). The reduction in particle velocity observed for the secondary wall CSC (**Fig. 4**) may be due to a similar effect. Although aggregation at sites within the bands of YFP–CSCs is not apparent, cessation of movement of plasma membrane-bound CSCs may feed-back to the delivery/recovery organelles directly below the secondary thickenings, resulting in a reduction of movement activity. As FLIP appears to measure organelle-type compartments, the observed changes in fluorescence decay may be a secondary effect of DCB. Alternatively, the mode of action of DCB could be different between the two types of cell wall.

In summary, a novel method is presented that uses FLIP to measure the speed of particles moving rapidly around a circular object. We have developed and used this method to examine the movement of CSCs in regions of secondary cell wall deposition in the developing xylem vessel. The speeds measured for movement of the CSC are hard to reconcile with simple movement of the CSC within the plasma membrane and suggest that a rapidly moving intracellular compartment exists directly below the secondary thickenings. The precise identification of these compartments is the subject of further study.

Materials and Methods

Plant growth conditions for microscopy

Seeds were surface sterilized in 30% (v/v) sodium hypochlorite solution containing 1% (v/v) Triton X-100 and washed five times in distilled water. Seeds were resuspended in 0.1% (w/v) agar (Sigma-Aldrich, Poole, UK) and spotted in lines on growth medium containing 2.2 g l^{-1} MS supplemented with Gamborg B5 vitamins (Duchefa, Haarlem, The Netherlands), 1.5% (w/v) agar, pH 6.8. Seeds were vernalized for 3 d at 4°C and then placed upright in a Gallenkamp environmental test chamber and incubated under constant light (~100 µmol m^{-2} s^{-1}) at 22°C. Whole seedlings were viewed under the confocal microscope after 5 d growth.

Fluorescence loss in photobleaching (FLIP)

FLIP was carried out on line RWY6a (Wightman and Turner 2008) using the FRAP tool of a Leica SP2 confocal microscope. The settings on the microscope were as follows: pinhole setting of 5.487 airy units, beam expander 3, zoom 4, unidirectional scanning with speed set to 800 Hz. Manual laser power control was set to maximum. Images were acquired using the 514 nm laser with a software laser power setting between 9 and 13%. Each experiment consisted of one pre-bleach scan, 40 bleach scans followed by 20 post-bleach scans. Bands located in regions exhibiting longitudinal transport of YFP-containing organelles were avoided. The bleach zone was applied during a bleach scan by raising the power of the 488, 496 and 514 laser lines to 100%. Seedlings treated with the cellulose synthesis inhibitor DCB (Dichlorobenil, Fisher Scientific) were mounted in 20 µM DCB in 0.1% (v/v) dimethylsulfoxide (DMSO). Untreated seedlings were mounted in 0.1% (v/v) DMSO. Mean pixel intensities were measured using ImageJ software (W. Rasband, NIH) and ImageSXM software (S. Barrett, University of Liverpool). For each scan, the sum of the FLIP bleach zone was subtracted from that of the whole band/hoop. General sample bleaching was measured by determining the mean pixel intensity of the xylem vessel in view minus the region undergoing FLIP. Hoop mean intensities were then normalized to general bleaching values. Surface plots were created using the 3D surface plot plugin of ImageJ (Kai Uwe Barthel, Internationale Medieninformatik, Germany). Images were contrast enhanced before surface plotting.

Statistical analysis comparing DCB-treated with untreated seedlings

Hoop mean pixel intensities were normalized to initial intensities (= 100%). Three-parameter exponential decay curves (Kaleidagraph, Synergy Software, Reading, PA, USA) were fitted to data from FLIP experiments carried out with bleach zones of ≤2 pixels wide. The relative intensity at the end of FLIP was used with values from other experiments to determine the average final intensity for DCB-treated and untreated seedlings. A Student's *t*-test was carried out using Excel based upon a two-tailed distribution, two-sample equal variance and an alpha value of 0.05. The *t*-test returned a value of 0.0026. The Mann–Whitney–Wilcoxon test returned values of $S = 31.5$, $Z = -2.92601$, $P = 0.0034$.

Measurements for velocity calculations

The radius and bleach zone width were measured using ImageJ software. Hoop mean intensities normalized to general acquisition bleaching were collated in Excel. All plots and trendlines were created in Kaleidagraph.

Fluorescent reporters of microtubules and the ER

RWYC2, expressing both *YFP–IRX3* and a CFP–microtubule reporter, has been previously described (Wightman and Turner 2008). For the ER reporter, the signal sequence (ss)–mCherry–HDEL fusion was constructed by PCR using a forward primer (ssCherry) containing the patatin signal sequence (5′-GCCGCTAGCATGGCAACTACTAAATCTTTTTTAATTTTATTTTTTATGATATTAGCAACTACTAGTTCAACAGTGAGCAAGGGCGAGGAGGATAACATGGCCATC-3′) and a reverse primer encoding the HDEL signal sequence (HDELchrev 5′-GCCTCTAGATTAAAGTTCATCCTTCTTGTACAGCTCGTCCATGCC-3′). The resultant DNA was cloned as a *Nhe*I–*Xba*I fragment into *Nhe*I–*Xba*I-cut pBluescript-EXFP-MBD-NosT (Wightman and Turner 2007). The construct was subcloned into the plant vector pCB1300 and transformed into line RWY6a to give RWYER1.

Supplementary data

Supplementary data are available at PCP online.

Funding

The Biotechnology and Biological Sciences Research Council (grant No. 34/C19282).

Acknowledgments

We thank Richard Preziosi for help with statistical analyses.

References

Ali, G.S., Prasad, K.V., Day, I. and Reddy, A.S. (2007) Ligand-dependent reduction in the membrane mobility of FLAGELLIN SENSITIVE2, an arabidopsis receptor-like kinase. *Plant Cell Physiol.* 48: 1601–1611.

Ali, G.S. and Reddy, A.S. (2006) ATP, phosphorylation and transcription regulate the mobility of plant splicing factors. *J. Cell Sci.* 119: 3527–3538.

Axelrod, D., Koppel, D.E., Schlessinger, J., Elson, E. and Webb, W.W. (1976) Mobility measurement by analysis of fluorescence photobleaching recovery kinetics. *Biophys. J.* 16: 1055–1069.

Cole, N.B., Smith, C.L., Sciaky, N., Terasaki, M., Edidin, M. and Lippincott-Schwartz, J. (1996) Diffusional mobility of Golgi proteins in membranes of living cells. *Science* 273: 797–801.

DeBolt, S., Gutierrez, R., Ehrhardt, D.W., Melo, C.V., Ross, L., Cutler, S.R., et al. (2007a) Morlin, an inhibitor of cortical microtubule dynamics and cellulose synthase movement. *Proc. Natl Acad. Sci. USA* 104: 5854–5859.

DeBolt, S., Gutierrez, R., Ehrhardt, D.W. and Somerville, C. (2007b) Nonmotile cellulose synthase subunits repeatedly accumulate within localized regions at the plasma membrane in Arabidopsis hypocotyl cells following 2,6-dichlorobenzonitrile treatment. *Plant Physiol.* 145: 334–338.

Delmer, D.P. and Amor, Y. (1995) Cellulose biosynthesis. *Plant Cell* 7: 987–1000.

Gardiner, J.C., Taylor, N.G. and Turner, S.R. (2003) Control of cellulose synthase complex localization in developing xylem. *Plant Cell* 15: 1740–1748.

Haigler, C.H. and Brown, R.M. (1986) Transport of rosettes from the Golgi apparatus to the plasma membrane in isolated mesophyll cells of Zinnia elegans during differentiation to tracheary elements in suspension culture. *Protoplasma* 134: 111.

Hepler, P.K. and Newcomb, E.H. (1964) Microtubules and fibrils in the cytoplasm of coleus cells undergoing secondary wall deposition. *J. Cell Biol.* 20: 529–532.

Herth, W. (1980) Calcofluor white and Congo red inhibit chitin microfibril assembly of Poterioochromonas: evidence for a gap between polymerization and microfibril formation. *J. Cell Biol.* 87: 442–450.

Herth, W. (1985) Plasma-membrane rosettes involved in localized wall thickening during xylem vessel formation of Lepidium sativum L. *Planta* 164: 12.

Mueller, S.C. and Brown, R.M., Jr., (1980) Evidence for an intramembrane component associated with a cellulose microfibril-synthesizing complex in higher plants. *J. Cell Biol.* 84: 315–326.

Paredez, A.R., Somerville, C.R. and Ehrhardt, D.W. (2006) Visualization of cellulose synthase demonstrates functional association with microtubules. *Science* 312: 1491–1495.

Reits, E.A. and Neefjes, J.J. (2001) From fixed to FRAP: measuring protein mobility and activity in living cells. *Nat. Cell Biol.* 3: 145–147.

Schneider, B. and Herth, W. (1986) Distribution of plasma membrane rosettes and kinetics of cellulose formation in xylem development of higher plants. *Protoplasma* 131: 142.

Somerville, C. (2006) Cellulose synthesis in higher plants. *Annu. Rev. Cell Dev. Biol.* 22: 53–78.

Taylor, N.G., Howells, R.M., Huttly, A.K., Vickers, K. and Turner, S.R. (2003) Interactions among three distinct CesA proteins essential for cellulose synthesis. *Proc. Natl Acad. Sci. USA* 100: 1450–1455.

Taylor, N.G., Laurie, S. and Turner, S.R. (2000) Multiple cellulose synthase catalytic subunits are required for cellulose synthesis in Arabidopsis. *Plant Cell* 12: 2529–2540.

Taylor, N.G., Scheible, W.R., Cutler, S., Somerville, C.R. and Turner, S.R. (1999) The irregular xylem3 locus of Arabidopsis encodes a cellulose synthase required for secondary cell wall synthesis. *Plant Cell* 11: 769–780.

Turner, S.R. and Somerville, C.R. (1997) Collapsed xylem phenotype of Arabidopsis identifies mutants deficient in cellulose deposition in the secondary cell wall. *Plant Cell* 9: 689–701.

Wey, C.L., Cone, R.A. and Edidin, M.A. (1981) Lateral diffusion of rhodopsin in photoreceptor cells measured by fluorescence photobleaching and recovery. *Biophys. J.* 33: 225–232.

White, J. and Stelzer, E. (1999) Photobleaching GFP reveals protein dynamics inside live cells. *Trends Cell Biol.* 9: 61–65.

Wightman, R. and Turner, S.R. (2007) Severing at sites of microtubule crossover contributes to microtubule alignment in cortical arrays. *Plant J.* 52: 742–751.

Wightman, R. and Turner, S.R. (2008) The roles of the cytoskeleton during cellulose deposition at the secondary cell wall. *Plant J.* 54: 794–805.

Wooding, F.B. and Northcote, D.H. (1964) The development of the secondary wall of the xylem in Acer pseudoplatanus. *J. Cell Biol.* 23: 327–337.

(Received October 6, 2008; Accepted January 27, 2009)